Nuclear Instruments and Methods in Physics Research A 607 (2009) 505–516

Contents lists available at ScienceDirect

Nuclear Instruments and Methods in Physics Research A

journal homepage: www.elsevier.com/locate/nima

Theory and application of plane elliptic multipoles for static magnetic fields

P. Schnizer [a,*], B. Schnizer [b], P. Akishin [c], E. Fischer [a]

[a] Gesellschaft für Schwerionenforschung, Darmstadt, Germany
[b] Technische Universität Graz, Austria
[c] Joint Institute for Nuclear Research, Dubna, Moscow Region, Russia

ARTICLE INFO

Article history:
Received 12 November 2008
Received in revised form
4 June 2009
Accepted 4 June 2009
Available online 12 June 2009

Keywords:
Static magnetic field reconstruction from numerical and measurement data
Field expansions
Plane elliptic multipoles
Plane circular multipoles
Magnetic measurement
Accelerator magnets

ABSTRACT

Standard textbooks on beam dynamics study the impact of the magnetic field quality on the beam using field representations based on circular multipoles. Iron dominated magnets, however, typically provide a good field region with a non-circular aspect ratio (i.e. an ellipse whose axis a is significantly larger than the axis b); a boundary not ideal for circular multipoles. The development of superconductors, originally driven to reach fields above ≈ 2 T, allows using them today in completely different fields: iron dominated DC magnets, to save the energy for coil powering as well as repeatedly fast ramped magnets. The cold mass of magnets, housed in common cryostats sectors, makes it tedious to implement additional correction magnets at a later stage, as it requires to warm up the sections where the magnets should be installed as well as unwelding the cryostat. Thus the field homogeneity of the magnets and its influence on the beam has to be thoroughly studied during the project planning phase.

Elliptic multipoles, a new type of field expansion for static or quasi-static (here magnetic) two-dimensional fields, are proposed and investigated, which are particular solutions of the potential equation in plane elliptic coordinates obtained by the method of separation. The proper subsets of these particular solutions appropriate for representing static real or complex fields regular within an ellipse are identified. Formulas are given for computing expansion coefficients from given fields. The advantage of this new approach is that the expansion is valid, convergent and accurate in a larger domain, namely in an ellipse circumscribed to the reference circle of the common circular multipoles in polar coordinates. Formulas are derived for calculating the circular multipoles from the elliptical ones. The effectiveness of the approach was tested on many different magnet designs and is illustrated here on the dipole design chosen for the core synchrotron (SIS 100) of the FAIR project as well as on measurement data obtained by rotating coil probes.

1. Introduction

Present-day accelerators, as, e.g. FAIR, apply superconducting magnets in places up to now reserved for conventional magnets. Superconducting magnets, as found in the SIS 100 synchrotron of FAIR, are housed in cryostats and are connected to each other by helium-tight weldings; thus inserting magnetic elements into the machine during commissioning or after a few years of operation is far more complicated than for a machine using conventional magnets.

This requires that the field in all aspects is fully understood during the R&D phase devoted to the machine project. The elliptical aperture, as foreseen for the SIS 100 synchrotron, the core component of the FAIR facility, motivated us to search for a consistent description of the magnetic field within the whole aperture, insensitive to artefacts created by numerical calculations or measurements.

The magnetic field of accelerator magnets, whose length is much bigger than the gap's transversal dimensions, are represented by a two-dimensional field following the thin lens approximation, if applicable, as found in light optics.

The magnetic field values computed by numerical methods or measured by field probes must be represented by an approximate analytical, but still sufficiently accurate, formula. Such a representation serves for quality checks, beam dynamics calculations a.s.o. The standard tool for representing a plane static magnetic field is an expansion w.r.t. circular multipoles $(r/R)^{|m|}e^{im\theta}, m = 0, \pm1, \pm2, \ldots$, see, e.g. Ref. [1]. r, θ are the common polar coordinates; the circle $r = R$, the reference circle, bounds the domain of this expansion. This domain is free of currents (i.e. free of current carrying wires, moving charges). The matter within this domain is assumed to be non-ferromagnetic with constant uniform permeability. Then the field is irrotational and may be derived from a static potential. This potential and both Cartesian field components are solutions of the potential equation. The

* Corresponding author. Tel.: +49 6159 71 1557.
E-mail addresses: p.schnizer@gsi.de (P. Schnizer), schnizer@itp.tu-graz.ac.at (B. Schnizer), akishin@jinr.ru (P. Akishin), e.fischer@gsi.de (E. Fischer).

0168-9002/$ - see front matter © 2009 Elsevier B.V. All rights reserved.
doi:10.1016/j.nima.2009.06.007

circular multipoles are just particular solutions of this partial differential equation.

If the cross-section of the gap is rectangular, then a circular domain fulfilling the conditions just listed will cover only a small part of the domain accessible to the beam. This is particularly noticeable if the cross-section of the beam is not circular but elliptic or a broad ribbon with an large aspect ratio. In such a case it is worthwhile to use an area bounded by an ellipse. The use of an area bounded by a rectangle is much less favourable since such a shape may penetrate a forbidden region (where there are currents) and it is more involved from the point of view of computations requiring four expansions in place of one.

In this paper we suggest to use expansions with respect to *elliptic multipoles*, which are particular solutions of the potential equation obtained by solving this partial differential equation in elliptic coordinates by the method of separation. These particular solutions are calculated and discussed; in particular it is pointed out that only a proper subset of all these solutions is needed. At the end it is shown in examples how much the field values found by evaluating the expansion differ from the field values due to the numeric field computation.

In the theory part of this paper the circular multipole expansion is given together with the formula for calculating the Fourier coefficients. This repetition of a well-known subject serves as a basis of comparison to the elliptic multipoles introduced thereafter. In the corresponding section the elliptical coordinates are described. Then the particular solutions of the potential equation in these coordinates and the elliptic multipole expansion are given. In the next section relations between circular and elliptic multipole coefficients are derived. At the end of this part we show how we used the formulas to check the consistency of field values computed by numeric methods.

In the applications part the field values obtained from numeric field computations are compared to the values calculated from the field expansions. Further a procedure is given to calculate the elliptic multipoles from measurements obtained using rotating coil probes and it is demonstrated using the measurement data obtained on the first SIS 100 dipole prototype.

Previous versions of these researches were circulated as internal notes. A very concise version was published in Ref. [2]. We believe that our results now are sufficiently mature to merit an extensive presentation.

2. Theory

The present investigation is limited to plane magnetic fields such as are found to a very good approximation in the inner part of a magnet, whose length is large as compared to the transverse dimensions of the field gap. From now on we reserve the term gap for this transverse cross-section. In this we select a domain where there are no field sources, such as charged particle beams or cables carrying currents; nor inhomogeneities of the permeability, which equals μ_0, that of the vacuum. A static field has no sources or vortices in this domain; so it may be derived from a scalar potential Φ_1 depending on the transversal coordinates only, say x,y; or polar coordinates r,θ; or the elliptic coordinates, η,ψ, which, will be defined below. This domain is simply connected; it is bounded by a closed curve, the reference curve, say, for example, by a rectangle, a circle or an ellipse. The potential Φ_1 and the Cartesian field components B_x and B_y are solutions of the two-dimensional Laplace equation, i.e. they are harmonic functions. This implies they are analytic functions, which are determined uniquely by their values along the reference curve.

We call multipoles regular particular solutions of the potential equation obtained by the method of separation of the independent variables. The general regular solution, which is capable of describing any static magnetic field in the domain, may be represented as a linear superposition of such particular solutions provided the set of functions is complete. Of course, it is impossible to work with an infinite number of functions in practice; still it is important to know this set; otherwise one may run into severe trouble or introduce more expansion parameters than necessary.

2.1. Circular multipoles

Circular multipoles are the common work horse for expansions of two-dimensional fields and are described in many books on accelerator theory or accelerator schools. We refer to Jain [1]. We quote a few properties, which are needed for comparisons with the elliptic multipoles.

Solving the Laplace equation in polar coordinates $0 \le r < \infty, -\pi \le \theta \le \pi$

$$x = r\cos\theta, \quad y = r\sin\theta \tag{1}$$

by assuming a solution of the type $\Phi_1 = R(r)\Theta(\theta)$ produces the following set of particular solutions:

$$\ln r, \quad r^m e^{im\theta}, \quad r^m e^{-im\theta}, \quad m = 0, \pm1, \pm2, \pm3, \ldots . \tag{2}$$

Omitting the functions singular at $r = 0$ we get the general solution of the potential equation regular within the circle $0 \le r \le R$ as

$$\Phi_1(r,\theta) = \Phi_0 \sum_{m=-\infty}^{\infty} c_m \left(\frac{r}{R}\right)^{|m|} e^{im\theta}. \tag{3}$$

The expansion coefficients c_m may be calculated by expanding a distribution $\Phi_1(r = R, \theta)$ given along the boundary with respect to the imaginary exponentials:

$$c_m = \frac{1}{2\pi}\int_{-\pi}^{\pi} \frac{\Phi(R,\theta)}{\Phi_0} e^{-im\theta}\, d\theta. \tag{4}$$

The imaginary exponentials ($e^{im\theta}, m = \text{integer} \in \{-\infty, \infty\}$) make up a complete system in the one-dimensional interval $-\pi \le \theta \le \pi$ as well as the set of trigonometric functions including a constant. In two dimensions the complex circular harmonics (2) as well as the real set

$$r^m\cos(m\theta), \quad r^m\sin(m\theta), \quad m = 0, 1, 2, 3, \ldots$$

make up a complete set within the circle $0 \le r \le 1$ [3]. One may also expand each of the real field components B_x and B_y with respect to circular multipoles or with respect to the trigonometric harmonics. But these two components are not independent, they must fulfil the two scalar conditions (here $\vec{e}_z$ is the normal to the field plane):

$$\operatorname{div}\vec{B} = 0 \ \text{(a)}, \quad \vec{e}_z \cdot \operatorname{curl}\vec{B} = 0 \ \text{(b)}. \tag{5}$$

These imply that the two sets of expansion coefficients as obtained from B_x and from B_y are not independent. So it is more convenient to combine the two real field components into a complex field.

2.1.1. The complex magnetic field

The two conditions given in the previous equation are the Cauchy–Riemann equations for the real part $B_y(x,y)$ and the imaginary part $B_x(x,y)$ of a complex function

$$\mathbf{B}(\mathbf{z}) := B_y + iB_x \tag{6}$$

of the complex variable

$$\mathbf{z} := x + iy = r\,e^{i\theta}. \tag{7}$$

The Cauchy–Riemann equations also restrict the set of complete functions to a proper subset of the circular harmonics used in (3); so the expansion of the field is now

$$\mathbf{B}(\mathbf{z})/\mathscr{B}_0 = \sum_{m=0}^{\infty} \mathbf{C}_m \left(\frac{r}{R}\right)^m e^{im\theta} = \sum_{m=0}^{\infty} \mathbf{C}_m \left(\frac{x+iy}{R}\right)^m. \tag{8}$$

$\mathscr{B}_0$ is the constant reference field value, which may be chosen conveniently. In the present work it is more convenient to use the US convention [1] for the field expansion. The expansion coefficients may be calculated from a complex field $\mathbf{B}_0(\theta) = \mathbf{B}(R\ e^{i\theta})$ given along the reference circle according to

$$\mathbf{C}_m = \frac{1}{2\pi}\int_{-\pi}^{\pi} \frac{\mathbf{B}_0(\theta)}{\mathscr{B}_0} e^{-im\theta}\, d\theta. \tag{9}$$

Circular multipoles with negative m give fields with sources and/or vortices. If a harmonic magnetic field is used in the preceding equation then the integrals assume zero value for negative m.

A complex potential $\mathbf{\Phi}(\mathbf{z})$ belonging to the magnetic field can be defined. Its real part is the real function $\Phi_1(x,y)$ related to the magnetic field by

$$\vec{B} = -\nabla\Phi_1(x,y) = -\left(\frac{\partial\Phi_1}{\partial x}, \frac{\partial\Phi_1}{\partial y}\right). \tag{10}$$

The corresponding imaginary part $\Phi_2(x,y)$ is found through the Cauchy–Riemann equations. The complex field is obtained from the complex potential by derivation with respect to the complex variable $\mathbf{z}$:

$$\mathbf{\Phi}(\mathbf{z}) := \Phi_1(x,y) + i\Phi_2(x,y), \quad \mathbf{B}(\mathbf{z}) = -\frac{d\mathbf{\Phi}}{d\mathbf{z}}. \tag{11}$$

2.2. Elliptic multipoles

In our new approach we propose to use an ellipse as reference curve since it permits one to cover a larger domain within a rectangular gap as compared to the area covered by a reference circle. This entails that we must use elliptic coordinates and elliptic multipoles.

2.2.1. Elliptic coordinates

Now the reference curve is an ellipse with the given semi-major axis a and the semi-minor axis b:

$$\frac{x^2}{a^2} + \frac{y^2}{b^2} = 1, \quad a > b. \tag{12}$$

A system of elliptic coordinates (Fig. 1) is defined according to Refs. [4,5] by

$$\begin{aligned} x &= e\cosh\eta\cos\psi, \quad 0 \le \eta < \infty \\ y &= e\sinh\eta\sin\psi, \quad -\pi \le \psi \le \pi. \end{aligned} \tag{13}$$

Varying ψ for fixed η gives an ellipse with semi-axes $e\cosh\eta > e\sinh\eta$. One gets a set of ellipses for all values of η in the range $0 < \eta \le \eta_0$, all belonging to the same foci $F, x = \pm e, y = 0$, whose elliptic coordinates are $\eta = 0, \psi = 0, \pm\pi$. These ellipses correspond to the circles $r = \text{const.}$ of the polar coordinates. The confocal hyperbolas, each belonging to a given ψ while η is varying, are orthogonal to all ellipses; they have semi-axes $e\cos\psi$ and $e\sin\psi$; they correspond to the radials $\theta = \text{const.}$ of the polar coordinates. There is an infinite set of elliptic coordinate systems. A particular system is specified by its value of the eccentricity e. The semi-axes of the reference ellipse determine the eccentricity e

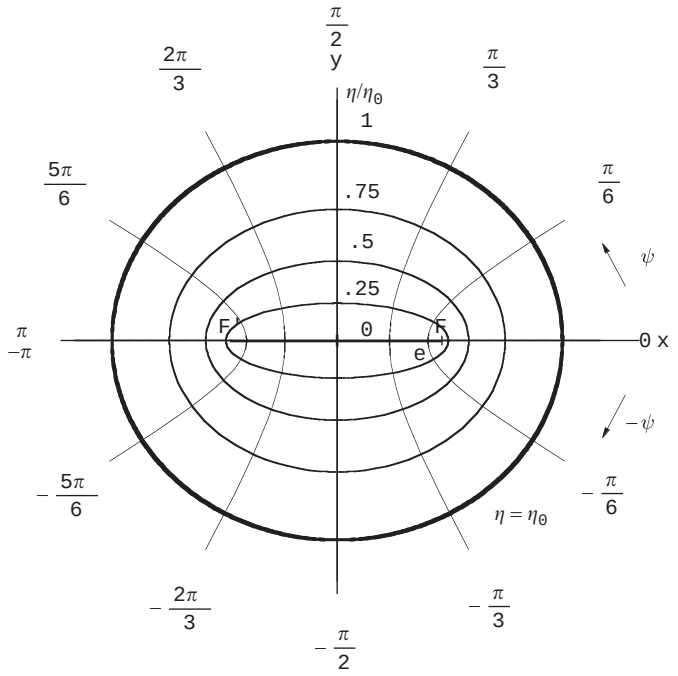

Fig. 1. Plane elliptic coordinates η, ψ, Foci F, F' are at $x = \pm e$.

and the corresponding value η_0:

$$\begin{aligned} &b = e\sinh\eta_0, \quad a = e\cosh\eta_0 \to \eta_0 = \tanh^{-1}(b/a). \\ &\varepsilon := \frac{e}{a} = \frac{\sqrt{a^2-b^2}}{a} = \sqrt{1-\tanh^2(\eta_0)}, \quad e = a\varepsilon. \end{aligned} \tag{14}$$

The easiest way to accomplish the transformation from the Cartesian to orthogonal curvilinear coordinates is by a conformal map [6]. The conformal map corresponding to (13) is

$$\begin{aligned} \mathbf{z} &= x + iy = e[\cosh\eta\cos\psi + i\sinh\eta\sin\psi] \\ &= e\cosh(\eta + i\psi) = e\cosh\mathbf{w} \end{aligned}$$

$$\mathbf{w} = \eta + i\psi = \text{Arcosh}(\mathbf{z}/e). \tag{15}$$

Note: Various authors use different letters for the elliptic coordinates. Even the definition of the plane elliptic coordinates is not always the same. For example, Ref. [6] uses $\mathbf{z} = e\sinh\mathbf{w}$ in place of (15).

The Laplacian in the elliptic coordinates as defined in (15) is

$$\Delta\Phi = \frac{1}{e^2(\cosh^2\eta - \cos^2\psi)}\left[\frac{d^2\Phi}{d\eta^2} + \frac{d^2\Phi}{d\psi^2}\right]. \tag{16}$$

The denominator in front of the derivatives is zero at the foci.

2.2.2. Real elliptic multipoles

Elliptic multipoles are defined as particular solutions, which are obtained from the potential equation $\Delta\Psi = 0$ by separation. The denominator of the operator in Eq. (16) is removed by multiplication. This gives a simple differential equation, whose solutions are obtained by separation. The ansatz $\Phi(\eta,\psi) = H(\eta)\bar{\Psi}(\psi)$ yields the two ordinary differential equations

$$\frac{d^2H}{d\eta^2} - \gamma H = 0 \quad \text{and} \quad \frac{\partial^2\bar{\Psi}}{\partial\psi^2} + \gamma\bar{\Psi} = 0.$$

Ψ must be periodic in ψ, so must be $\bar{\Psi}$. This implies $\gamma = m^2$, $m = \text{integer} \neq 0$. This in turn leads to hyperbolic functions

for the solutions H:

$$\bar{\Psi}_m(\psi) = e^{im\psi}, \quad m = \pm1, \pm2, \pm3, \ldots \tag{17}$$

$$H_m(\eta) = a_m \cosh(m\eta) + b_m \sinh(m\eta). \tag{18}$$

For $m = 0$ we get

$$\bar{\Psi}_0 = 1; \quad H_0(\eta) = a_0 + b_0\eta. \tag{19}$$

So the most general solution may be written as

$$\Psi_g(\eta,\psi) = a_0 + b_0\eta + \sum_{m=-\infty}^{m=\infty'} [a_m \sinh(|m|\eta) + b_m \cosh(|m|\eta)]\, e^{im\psi}. \tag{20}$$

The primed sum does not contain a term with $m = 0$. b_0 must be zero for the following reason. The product $H_0(\eta)\bar{\Psi}_0$ is a harmonic function, which is constant on the boundary, the reference curve, the ellipse $\eta = \eta_0$. So it must be constant everywhere within the boundary according to a general theorem of potential theory [7]. If we try to calculate the expansion coefficients in Eq. (20) from values of the potential given along the boundary, the reference ellipse $\eta = \eta_0$ we encounter a difficulty. Using the orthogonality of the $e^{im\psi}$ we find for integer $m \neq 0$:

$$a_m \sinh(|m|\eta_0) + b_m \cosh(|m|\eta_0) = \frac{1}{2\pi}\int_{-\pi}^{\pi} \Psi(\eta_0,\psi)\, e^{-im\psi}\, d\psi.$$

So we do not have enough conditions to determine all a_m and b_m. The way out from this impasse is that not all functions written down in Eq. (20) are really needed. Below it will be shown that the complete system of *elliptic multipoles for the potential equation* consists of the following terms only:

$$1; \quad \cos(m\psi)\cosh(m\eta), \quad \sin(m\psi)\sinh(m\eta); \quad m = 1, 2, 3, \ldots. \tag{21}$$

So it is entirely correct to use the following expansion for any harmonic function within the reference ellipse:

$$\Psi(\eta,\psi)/\Psi_0 = \frac{a_0}{2} + \sum_{n=1}^{\infty}\left[a_n \frac{\cosh(n\eta)}{\cosh(n\eta_0)}\cos(n\psi) + b_n \frac{\sinh(n\eta)}{\sinh(n\eta_0)}\sin(n\psi)\right]. \tag{22}$$

The expansion coefficients may be determined from boundary values $\Psi(\eta_0,\psi)$ given along the reference ellipse $\eta = \eta_0$:

$$a_n = \frac{1}{\pi}\int_{-\pi}^{\pi} \frac{\Psi(\eta_0,\psi)}{\Psi_0}\cos(n\psi)\, d\psi, \qquad b_n = \frac{1}{\pi}\int_{-\pi}^{\pi} \frac{\Psi(\eta_0,\psi)}{\Psi_0}\sin(n\psi)\, d\psi. \tag{23}$$

The complete system (21) consists of products comprising either even or odd functions but no mixed products. This may be seen from the Green's function of the potential equation in elliptic coordinates given in Ref. [5]. An independent proof starts from the circular multipoles expressed in Cartesian coordinates. Inserting the transformation formulas (13) and transforming the powers of the trigonometric and the hyperbolic functions into harmonics gives only functions belonging to the set (21). For example:

$$\begin{aligned} 4\,\mathrm{Re}((x+iy)^3) &= 4x^3 - 12xy^2 \\ &= e^3[3\cosh(\eta)\cos(\psi) + \cosh(3\eta)\cos(3\psi)] \\ 4\,\mathrm{Im}((x+iy)^3) &= 12x^2y - 4y^3 \\ &= e^3[3\sinh(\eta)\sin(\psi) + \sinh(3\eta)\sin(3\psi)]. \end{aligned}$$

Inspection of these examples reveals that the conversion of the circular multipoles by the insertion of elliptic coordinates produces only linear combinations of the elliptic multipoles listed in (21). The general law follows from the working of the various powers of the imaginary unit and of the addition theorems of the trigonometric and hyperbolic functions as exemplified in the derivation of Moivre's formulas.

2.2.3. Complex elliptic multipoles

As shown in Section 2.1.1, source-free irrotational plane magnetic fields may be combined to a complex field, whose expansion involves only circular harmonics with non-negative m's. The same reasons restrict the expansion of the complex field with respect to elliptic multipoles to a subset of those given in (21). So we can define the following expansion of the complex field with respect to complex elliptic multipoles:

$$\mathbf{B}/\mathscr{B}_0 = \frac{\mathbf{E_0}}{2} + \sum_{n=1}^{\infty}\mathbf{E}_n \frac{\cosh[n(\eta + i\psi)]}{\cosh(n\eta_0)}. \tag{24}$$

The convergence of this series can be estimated from the following estimates:

$$\left|\frac{\cosh[n(\eta+i\psi)]}{\cosh(n\eta_0)}\right| = \sqrt{\frac{\cos(2n\psi)+\cosh(2n\eta)}{1+\cosh(2n\eta_0)}} \tag{25}$$

$$\leq \frac{\cosh(n\eta)}{\cosh(n\eta_0)} \sim e^{-n(\eta_0-\eta)}. \tag{26}$$

So the elliptic multipoles decrease exponentially with growing order n within the reference ellipse. On the circumference the elliptic multipoles have absolute value unity; so the decay of the coefficients $\mathbf{E}_n$ is decisive for the convergence; which behaviour depends on the continuity of the field components and their derivatives on the curve. The Fourier coefficients may be computed from values of a proper complex field given along the reference ellipse $\eta = \eta_0$ according to

$$\mathbf{E}_n = \frac{1}{\pi\mathscr{B}_0}\int_{-\pi}^{\pi} \mathbf{B}_0(\mathbf{z} = e\cosh(\eta_0 + i\psi))\cos(n\psi)\, d\psi \tag{27}$$

$$= \frac{1}{2\pi\mathscr{B}_0}\int_{-\pi}^{\pi} [\mathbf{B}_0(\mathbf{z} = e\cosh(\eta_0 + i\psi)) + \mathbf{B}_0(\mathbf{z} = e\cosh(\eta_0 - i\psi))]\, e^{in\psi}\, d\psi. \tag{28}$$

The completeness of expansion (24) follows from Eq. (8) by inserting the transformation (15):

$$\mathbf{B}(\mathbf{z})/\mathscr{B}_0 = \sum_{m=0}^{\infty}\mathbf{C}_m\left(\frac{x+iy}{R}\right)^m = \sum_{m=0}^{\infty}\mathbf{C}_m\alpha^m\cosh^m\mathbf{w} \tag{29}$$

with

$$\alpha := e/R. \tag{30}$$

Now, any non-negative integer power of $\cosh^m x$ can be decomposed into harmonics $\cosh(mx)$ with non-negative integers m [8]. This transforms the circular expansion into the elliptic expansion comprising only terms with $\cosh(n\mathbf{w})$.

2.3. Relations between circular and elliptic multipoles

Magnet quality criteria are based on circular multipole expansions. Beam dynamics programs work with these. So linear transformations are needed which permit one to switch from the elliptic expansion to the circular one.

2.3.1. Relations between coefficients of the complex field expansions

It is easy to find the relations between the expansion coefficients of the complex magnetic field. These are derived by equating the field expansions (24) and (29). Using the orthogonality of the $\cos(n\psi)$ we get

$$\bar{\mathbf{E}}_n := \mathbf{E}_k/\cosh(k\eta_0) = \sum_{m=0}^{\infty}\mathbf{C}_m\alpha^m s_{mk} \tag{31}$$

with

$$s_{mk} = \delta_{m+k,\text{even}} \frac{1}{2^{(m-1)}} \binom{m}{(m-k)/2}, \quad k, m = 0, 1, 2, \ldots \tag{32}$$

and

$$\delta_{m+k,\text{even}} := [1 + (-1)^{m+k}]/2. \tag{33}$$

The integrals over ψ can be calculated by use of the binomial theorem [9] or found in Ref. [8]. The binomial coefficient is undefined if the lower argument is not a non-negative integer. But in this case $\delta_{m+k,\text{even}}$ is zero. This entails that every second element of the matrix S is zero and that the even/odd parity of k and m is the same on both sides of the linear transformations given above and below. The matrix S is a lower triangular one since all binomial coefficients with $k > m$ are zero.

The inverse transformation is

$$\alpha^m \mathbf{C}_m = \sum_{k=0}^{\infty} \mathbf{E}_k / [(1 + \delta_{k0}) \cosh(k\eta_0)] t_{km}, \quad k, m = 0, 1, 2, \ldots . \tag{34}$$

The matrix $T = (t_{km}) = \tilde{S}^{-1}$ is the transposed inverse of the matrix $S = (s_{mk})$. It is an upper triangular matrix; in addition every second element of it is zero. T may be found by analytic or numeric inversion of the matrix S or from the formula:

$$t_{ns} = \text{Res}(\sinh \mathbf{w} \cosh(n\mathbf{w}) / \cosh^{s+1} \mathbf{w}, \mathbf{w} = \mathbf{w}_0 = i\pi/2). \tag{35}$$

The operator Res denotes the residue of the function given in the first argument of the pole $\mathbf{w} = \mathbf{w_0}$ as it is defined in the theory of complex analytic functions. Formula (35) is derived below; it is easily evaluated for a given value s by computer algebra. Doing this for a few even and odd values of s gives enough insight so that one can guess the general structure, which leads to the following expressions substantiated by numerous checks:

$$m = \text{even}: \; t_{km} = (-1)^{m/2} \cos(k\pi/2) \frac{1}{m!} \times \Pi_{\mu=1}^{m/2} (k^2 - [2(\mu - 1)]^2) \tag{36}$$

$$m = \text{odd}: \; t_{km} = (-1)^{(m-1)/2} \sin(k\pi/2) \frac{k}{m!} \times \Pi_{\mu=1}^{(m-1)/2} (k^2 - (2\mu - 1)^2). \tag{37}$$

Peña and Franchetti [9] also investigated the elliptic multipoles as proposed by us. They also found recurrence formulas for a matrix expressing the circular by linear combinations of the elliptic expansion coefficients. This matrix accomplishes the same task as our matrix T. The expressions and values of our and their transformation matrices differ somewhat on account of different definitions.

The relations derived above give analytic expressions of the transformation matrices for any integer k and m. In principle, these indices may be as large as one pleases. The limited accuracy of the numerical or experimental results will restrict the number of terms in the field expansions, (8) and (24), so the upper values of m and n in practice. The same applies to the ratio α. This means one cannot extrapolate from points within the reference curve to points far outside the reference curve.

Eq. (35) is found from a slightly modified form of the equality of expansions (24) and (29):

$$\sum_{m=0}^{\infty} \mathbf{C}_m \mathbf{z}^m = \frac{\bar{\mathbf{E}}_0}{2} + \sum_{n=1}^{\infty} \bar{\mathbf{E}}_n \cosh(n\mathbf{w}). \tag{38}$$

Both sides of this equality are divided by z^{s+1}, the resulting expression is integrated over z along a closed curve $\mathscr{C}_z$ surrounding the origin $z = 0$. By Cauchy's residue theorem we get $2\pi i \mathbf{C}_s$ from the left-hand side. So this operation singles out one and only one coefficient from the $\mathbf{C}_m$'s. In the integrals on the right-hand side the variable $\mathbf{z}$ is replaced with the mapping function $\mathbf{z} = e \cosh \mathbf{w}, d\mathbf{z} = e \sinh \mathbf{w}\, d\mathbf{w}$. This transformation maps the

Table 1
Conversion matrices for two different ellipses.

m	k									
	0	1	2	3	4	5	6	7	8	9
$a = 5.75$, $b = 3.0$, $R = 4.0$										
0	0.50		−0.57		0.20		−0.06		0.02	
1		0.70		−0.84		0.45		−0.20		0.08
2			0.76		−1.04		0.74		−0.42	
3				0.74		−1.20		1.06		−0.71
4					0.69		−1.32		1.38	
5						0.64		−1.41		1.70
6							0.58		−1.47	
7								0.53		−1.51
8									0.49	
9										0.45
$a = 4.5$, $b = 1.7$, $R = 4.0$										
0	0.50		−0.75		0.39		−0.18		0.08	
1		0.89		−1.60		1.29		−0.83		0.48
2			1.38		−2.89		3.03		−2.45	
3				1.97		−4.76		6.11		−5.93
4					2.66		−7.45		11.29	
5						3.51		−11.26		19.68
6							4.58		−16.65	
7								5.93		−24.19
8									7.67	
9										9.91

The different factors are given rounded to two digits after the comma. All factors exactly zero are left out.

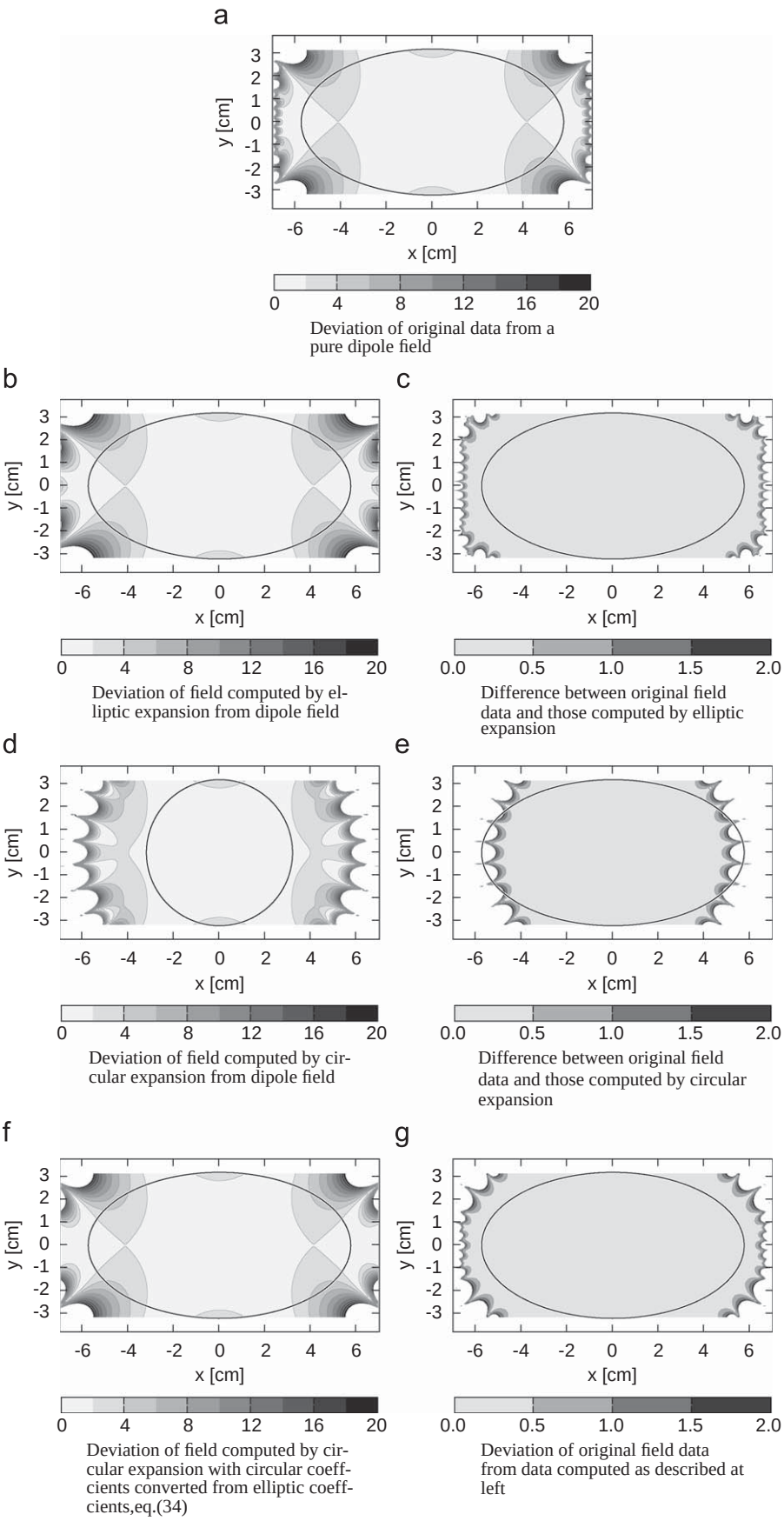

Fig. 2. Test of the interpolation for the CSLD8b at a current of 873 A and a field of 0.13 T. The field B_y in the aperture is plotted. The gray indicates the absolute value of the deviation (in units). The original data are given on top. The left column shows the data as reconstructed using the interpolation and the right columns shows the absolute value of the difference between the reconstructed and the original data.

origin $\mathbf{z}=0$ on $\mathbf{w}_0=i\pi/2$; the curve $\mathscr{C}_z$ on a closed curve $\mathscr{C}_w$ around $\mathbf{w}_0$. We get

$$2\pi i\mathbf{C}_s = 2\pi i\frac{\bar{\mathbf{E}}_0}{2}t_{0s} + \sum_{n=1}^{\infty} 2\pi i\bar{\mathbf{E}}_n t_{ns}$$

with

$$2\pi i t_{ns} = \oint_{\mathscr{C}_w} d\mathbf{w}\sinh\mathbf{w}\cosh(n\mathbf{w})/\cosh^{s+1}\mathbf{w}.$$

The integral above has a pole of order $s+1$ at $\mathbf{w}_0$, in general. Its value is equal to $2\pi i$ times the residue of the integrand at the pole $\mathbf{w}_0$. This is just Eq. (35).

For numerical evaluation Eq. (34) can be rewritten to

$$\mathbf{C}_m = \sum_{k=0}^{\infty} \underbrace{\frac{t_{km}/(1+\delta_{k0})}{\cosh(k\eta_0)\alpha^m}}_{T_{mk}}\mathbf{E}_m \tag{39}$$

and calculated by a matrix vector multiplication (T_{mk} is the full ratio). The matrix coefficients T_{mk} are presented for two different ellipses in Table 1, with the first one used for calculating circular harmonics from numeric field data (see Section 3) while the second one is used for calculating circular multipoles from measurement data (see Section 4). One can see that the matrices are an upper triangle matrix as well as that all coefficients are real numbers. The second matrix presented is for an ellipse with an larger aspect ratio. One can see that for the first one the coefficients in the trace are decreasing for larger k, m while they are increasing for larger k, m for the second ellipse. Second the off diagonal elements are larger for the second ellipse. Thus an elliptic multipole of a certain amplitude will be converted to larger coefficients for the second ellipse.

2.3.2. Relations between coefficients of the expansions for the potential

The expansions of the potential of a two-dimensional static field, which is not source-free, with respect to circular and to elliptic multipoles, i.e. Eqs. (3) and (22), comprise more terms as given in Eqs. (31), (34) or (38). Still the coefficients are related to each other. The corresponding equations may be derived by equating these two series, Eqs. (3) and (22)—while assuming $\Phi_0=\Psi_0$—and by evaluations similar to those used in the previous subsubsection. So we give just the results. The matrices S and T are the same as above. The coefficients of the elliptic multipoles are expressed by the circular ones as

$$a_k = \cosh(k\eta_0)\sum_{m=0}^{\infty}\alpha^m s_{mk}(c_m + c_{-m}) \tag{40}$$

$$b_k = \sinh(k\eta_0)\sum_{m=0}^{\infty}\alpha^m s_{mk} i(c_m - c_{-m}). \tag{41}$$

The coefficients of the circular multipoles are expressed by the elliptic ones as

$$c_0 = \frac{a_0}{2} + \sum_{k=1}^{\infty}(-1)^k\frac{a_{2k}}{\cosh(2k\eta_0)} \tag{42}$$

$$\alpha^m c_{\pm m} = \frac{1}{2}\sum_{k=0}^{\infty} t_{|m|k}\left[\frac{a_k}{\cosh(k\eta_0)} \mp \frac{ib_k}{\sin(k\eta_0)}\right], \quad m=1,2,3,\ldots. \tag{43}$$

3. Application on calculated fields

The formulae described in the previous chapters are now applied to dipole fields to demonstrate that all these steps are necessary to interpolate the field within the ellipse with a precision of better than the maximum tolerable field deviation

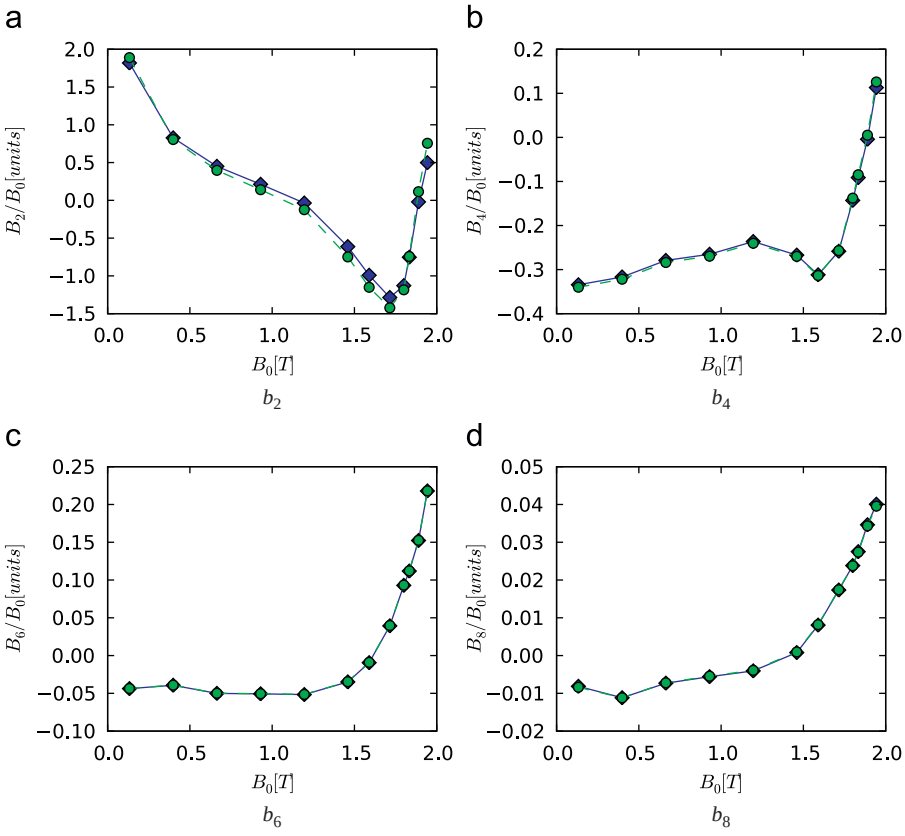

Fig. 3. The field quality for the 8 turn curved single layer dipole version b (CSLD-8b) The solid line gives the multipoles as obtained from the elliptic multipoles and the dashed line as calculated on a circle. Please note that the changes are small but significant (e.g. sextupole, difference in the order of 0.2 units). (a) b_2. (b) b_4. (c) b_6 (d) b_8.

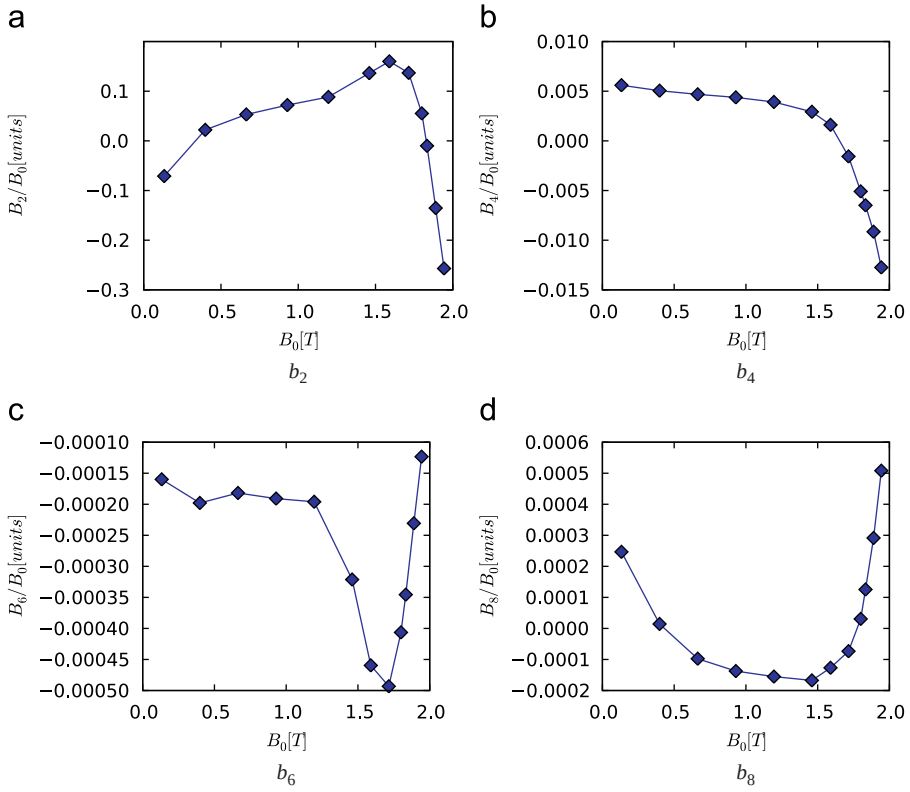

Fig. 4. The difference between the coefficient sets for the 8 turn curved single layer dipole version b (CSLD-8b). The circular ones calculated from the data on the circle were subtracted form the circular ones obtained from the elliptic ones. (a) b_2, (b) b_4, (c) b_6 and (d) b_8.

of 600 ppm or six units (one unit corresponds to 100 ppm). Mathematically speaking the field quality $\mathbf{\Delta B}$ of a dipole (in units) is given by

$$\mathbf{\Delta B(z)} = \frac{\mathbf{B(z)} - \mathbf{B(0)}}{\mathbf{B(0)}} 10^4. \tag{44}$$

The higher order harmonics (for the dipole) are given by

$$b_n + ia_n = \mathbf{c}_n = \frac{\mathbf{C_n}}{\mathbf{C_0}} 10^4. \tag{45}$$

The field quality was calculated for the curved single layer dipole with 8 turns [2,10], the dipole design chosen for the main dipole for the SIS 100 machine of FAIR. The original distribution is given in Fig. 2(a) at a current of 873 A yielding a field of ≈ 0.13 T. The field was taken along the ellipse and the elliptic multipoles were calculated as defined in Eq. (28). Using the first 20 coefficients the field was interpolated within the aperture (see Fig. 2(b)). The naked eye cannot see any difference to the original data (Fig. 2(a)). The original field was subtracted from the interpolated one. One can see from Fig. 2(c) that this difference is well below half a unit and thus sufficiently precise. Normally circular multipoles are used. So we calculated them using a Fourier transform of the data along a circle. Again the interpolation data was calculated (see Fig. 2(d)) and the difference to the original data (see Fig. 2(e)) using the first 15 coefficients. One can see that the interpolation works well within the circle but outside the circle soon the errors get unacceptably large. The difference outside of the circle is even larger if more coefficients are used. At last the circular multipoles were calculated from the elliptic ones as described in Eq. (34) (see Fig. 2(f) for the interpolation and Fig. 2(g)) for the difference). One can see that contrary to the row above the interpolation works even outside the circle and within the whole ellipse.

So the plots of Fig. 2 show that the interpolation based on the elliptic representation is mandatory to achieve an interpolation with sufficient accuracy; thus it is interesting to see how large the difference is. This is illustrated for the allowed circular harmonics of the aforementioned dipole along the load line (i.e. at different current points within the typical operation limits) in Fig. 3. The largest difference is found for the sextupole b_2 and is in the order of 0.2 units (= 20 ppm). For all higher multipoles it is not visible in this scale. Thus the difference is shown for all of them in Fig. 4. So except for the sextupole the difference is less then 1 ppm!

When choosing one magnet design amongst different designs one could compare plots of the field deviation for each magnet. These are, however, misleading and thus it is often preferred to compare the strength of the higher order harmonics along the load line for the different designs. This is illustrated using the aforementioned dipole design CSLD-8 and an alternative single layer dipole version with 10 turns as proposed in Ref. [11]. The circular multipoles and the circular ones calculated from the elliptic ones are given for both designs (see Fig. 5). Here one can clearly see that, although the sextupole strength is lower for the CSLD-10 for low fields than that of the CSLD-8b, the strengths are much larger for all other harmonics and also for the sextupole for medium or high field strengths. Thus the CSLD-8b is clearly the better field design and therefore rightfully chosen as the base design for the main dipole of SIS 100.

The same was done for various quadrupole designs. Given that the currently available two-dimensional designs and associated calculations have allowed harmonics less than one unit such illustrations were omitted here as they only show the limits of the field calculations and artefacts not to be found in a real magnet.

4. Application on measurements

The first full size SIS 100 magnet has been built [12–15] and the magnetic field was measured using a rotating coil probe [16],

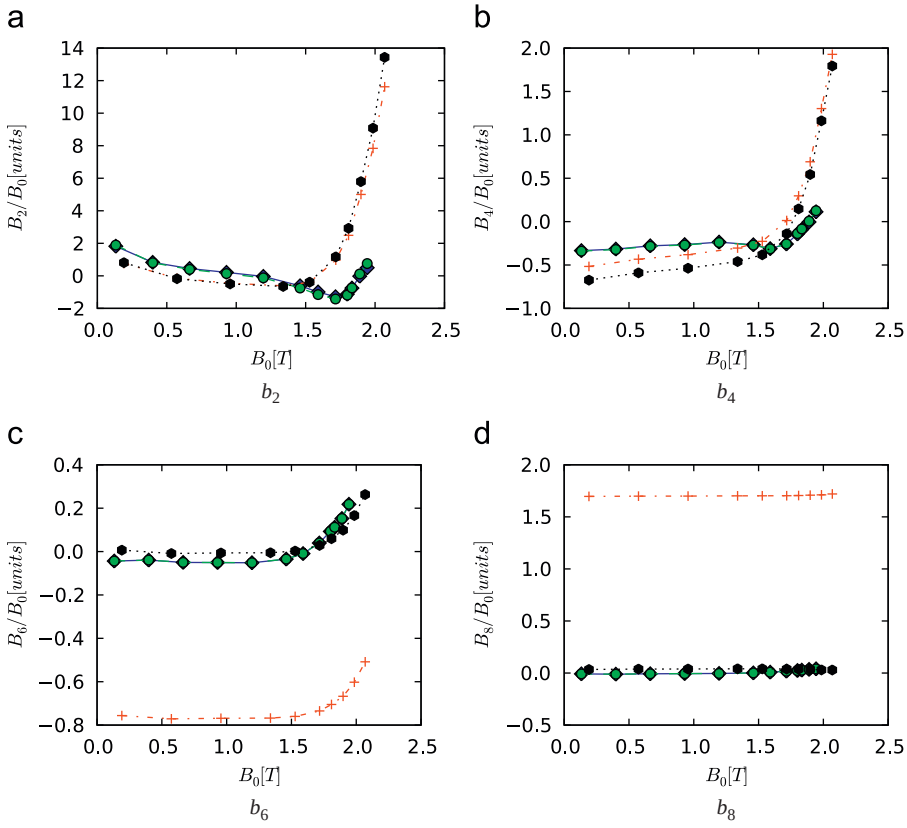

Fig. 5. The field quality for the 8 turn curved single layer dipole version (CSLD-8b) compared to the field quality of the 10 turn design. The solid line gives the multipoles as obtained from the elliptic multipoles and the dashed line as calculated on a circle for CSLD-8b. The dash-dotted line gives the multipoles as obtained from the elliptic multipoles and the dotted line as calculated on a circle for the 10 turn version. (a) b_2, (b) b_4, (c) b_6 and (d) b_8.

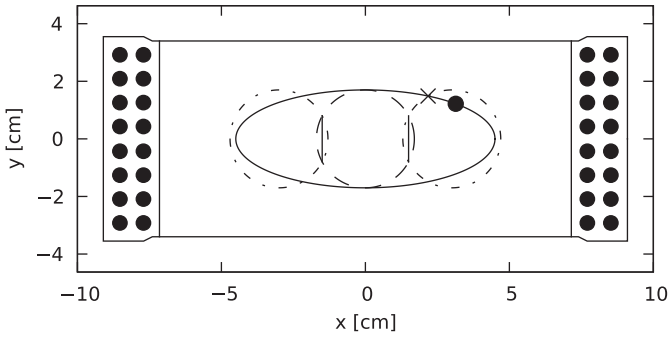

Fig. 6. The gap of the measured magnet as well as the measurement positions of the coil probe. The 16 black circles on the left and on the right indicated the 16 turns of the magnet's coil windings. The circles indicate the different positions of the measurements (dashed centre circle, dashed dotted circle $x_m = \pm 3.0\,\mathrm{cm}$) and the ellipse indicates where the field is reconstructed. The solid line indicates the ellipse used in the reconstruction. The solid dot on the ellipse indicates the angle ψ_p.

equipped with bucking coil probes. Now the procedure of calculating the elliptic and circular multipoles from measurement data is demonstrated for the end field as measured when the magnet was powered to a field level of approximately 0.22 T. The end field is chosen for this demonstration as it is much more inhomogeneous than the field in the centre of the magnet. Thus measurement errors are less contributing to the field deterioration, as the used system is dominated by absolute errors, and therefore the strengths and weaknesses of the multipoles are shown.

The magnet's gap is $12.5 \times 6.8\,\mathrm{cm}^2$. As this magnet is superconducting and thus operated at $\approx 4.5\,\mathrm{K}$ an anticryostat was used, which limits the space accessible within the magnet. The magnetic field was measured at three different lateral positions ($x_m = 0, \pm 3.0\,\mathrm{cm}$) with a rotating coil probe of 1.7 cm radius (see Fig. 6). Thus for the ellipse the axes were chosen as $a = 4.5\,\mathrm{cm}$ and $b = 1.7\,\mathrm{cm}$. For calculating the elliptic multipoles the field on the ellipse has to be reconstructed from the multipoles $\bar{\mathbf{C}}_\mathbf{m}^{\mathbf{l,c,r}}$ as obtained by the measurements at $x_m = -3.0$ (left one indicated with l), at $x = 0$ (centre one, indicated with c) and at $x_m = 3.0$ (right one indicated with r). The used coil probe was long enough to cover the whole end field so that at both ends of the probe $B_z = 0$.

The field direction of the measurement was not available. In a first step all multipoles were rotated to cancel the skew dipole (i.e. so that the dipole field coincides with the vertical axis). Now the field was calculated along the ellipse using the multipoles $\bar{\mathbf{C}}_\mathbf{m}^\mathbf{r}$ for the circumference the ellipse is within the area covered by the measurement at the right; similarly the multipoles $\bar{\mathbf{C}}_\mathbf{m}^\mathbf{l}$ were used for the circumference of the ellipse within the area covered by the measurement at the left side; finally the multipoles $\bar{\mathbf{C}}_\mathbf{m}^\mathbf{c}$ are used for the rest of the circumference (see Fig. 7). The discontinuity between the coil measurements has to be treated before any multipoles can be calculated.

As the coil probe is equipped with dipole bucking windings, the field variation can be determined with a significantly higher accuracy than the main dipole field (field strength $|\mathbf{C_0}|$ as well as field angle $\arg(\mathbf{C_0})$) [17,18]. Thus the field was calculated in the intersections (indicated by the dashed lines in Fig. 6). So for these intersections the two measurements covering the intersecting area must reproduce the same field. This is not the case for the measured data. Thus two optimisation parameters g and β were introduced as well as the function

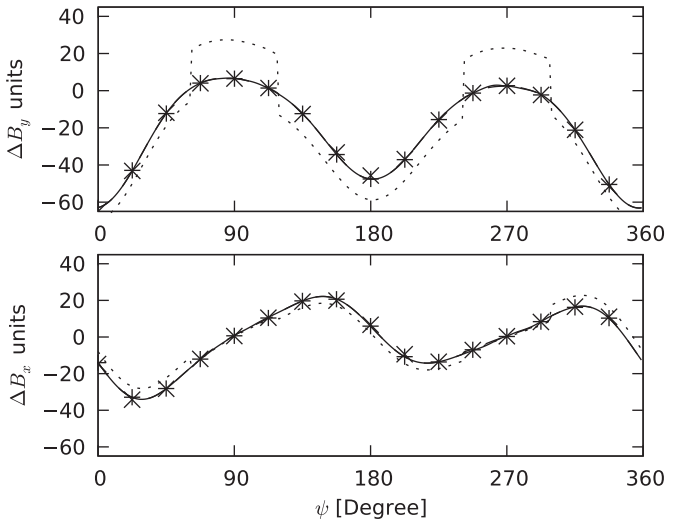

Fig. 7. The field as recalculated from the measurement at a central field level of ≈ 0.22 T. The dotted line shows the field as calculated from the measurement data without artefact removal, the dashed line the field as calculated form the measurement data after adjusting the multipoles according to the procedure described in the paragraph around Eq. (46) and the solid line when the weight function λ is used. The dashed line coincides nearly with the solid lines (a difference is only visible of ΔB_x at $\psi \approx 270^\circ$. The plus symbols show the field reconstructed using the elliptic multipoles and the cross-symbols when using the circular multipoles calculated from the elliptic ones.

$$\mathbf{C}_m = \left(1 + \frac{g}{10\,000}\right)\bar{\mathbf{C}}_\mathbf{m}\, e^{i(m+1)\beta} \tag{46}$$

to correct the measured multipoles $\bar{\mathbf{C}}_\mathbf{m}$. The factor g is a model of the accuracy limitation of the signal acquisition electronics. When measuring the end field the integrated field strength seen by the coil probe depends strongly on the longitudinal position and thus g also allows to compensate errors due to imperfections in positioning the coil probe longitudinally. β is motivated by the fact that the field direction for the measurements does not necessarily need to be identical for all three measurements. $g^{l,c,r}$ and $\beta^{l,c,r}$ were chosen such that the square of the field difference was minimised along the intersections (as indicated as small solid lines in Fig. 6). g was found to be typically less than 5 in the centre of the magnet and thus within the expected accuracy achieved by the used rotating coil measurement system and β was typically less than 1 mrad. For the measurement of the magnet end g was in the order of 20, which can be explained by the limited longitudinal coil probe positioning accuracy.

After these minimisations the fields at the edge are still discontinuous with steps in the order of up to one unit. So the field data of the two adjacent measurements shall be intermixed by a function λ, thus the interpolated field $\mathbf{B_i}(\mathbf{z})$ shall be given by

$$\mathbf{B_i}(\mathbf{z}) = \lambda \sum_{m=0}^{M_m} \mathbf{C_m^c}\left(\frac{\mathbf{z}}{R_m}\right)^m + (1-\lambda)\sum_{m=0}^{M_m} \mathbf{C_m^{l,r}}\left(\frac{\mathbf{z}-x_m}{R_m}\right)^m \tag{47}$$

with R_m the measurement radius. M_m was chosen to be 10. To define lambda, the measurement error and thus the weight $w^{l,c,r}$ of the appropriate multipoles at any point z is estimated by the distance of the point of interest from the centre of rotation of the coil probe, so that

$$w^l = \frac{R_m}{|\mathbf{z}-x_m|}, \quad w^c = \frac{R_m}{|\mathbf{z}|}, \quad w^r = \frac{R_m}{|\mathbf{z}+x_m|} \tag{48}$$

and λ^{cl} and λ^{cr} could be chosen to

$$\lambda^{cl} = \frac{w^c}{(w^c+w^l)}, \quad \lambda^{cr} = \frac{w^c}{(w^c+w^r)}. \tag{49}$$

Given that the weights $w^l,\ldots,w^r$ are not much larger than one and the weight in the area in question is almost linear (see Fig. 8), λ is not modelled as given above but chosen to enforce a continuous $\mathbf{B_i}(\mathbf{z})$ and first derivative. Thus λ is given by

$$\lambda(p_0)=0, \quad \lambda(p_1)=1, \quad \lambda'(p_0,p_1)=0, \quad \lambda(p)=3p^2-2p^3 \tag{50}$$

with

$$p = \begin{cases} 0, & \psi < p_0 \\ \dfrac{2\psi-\pi}{2p_0-\pi}, & p_0 \le \psi \le \pi. \end{cases} \tag{51}$$

for the first quadrant. p for the other quadrants can be calculated after reducing the angle to the first quadrant. One could use $p_0=\psi_c$, i.e. the angle at which the ellipse intersects the circle, as the authors proposed in Ref. [2]. But if one plots the weight

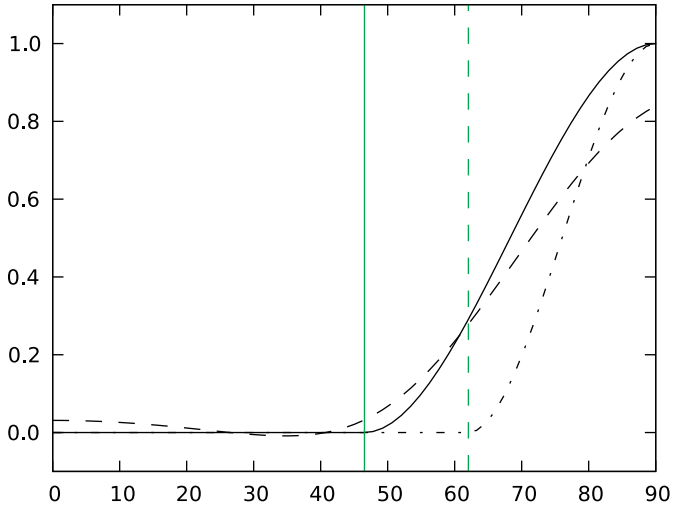

Fig. 8. The weights of the measurement as well as the interpolation functions versus the angle ψ for the first quadrant. The solid line indicates the function λ with $p_0 = 0.75\psi_c$ and the dashed dotted line the function λ with $p_0=\psi_c$. The dashed line indicates the weight function for the measurement in the centre $2\lambda^{cr}-0.5$. The scale and offset are used to facilitate the visual comparison to the function λ. The vertical dashed line indicates the angle ψ_c and the vertical solid line the angle $p_0 = 0.75\psi_c$.

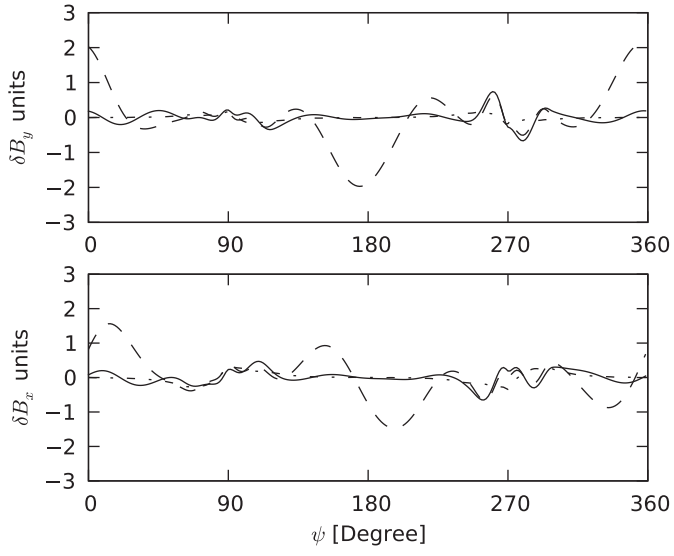

Fig. 9. The field interpolation errors for the elliptic using the first eight coefficients (solid line), for the circular representation using seven coefficients (dashed line) and for the circular representation using 30 coefficients (dash-dotted line).

functions one can see that $p_0 = 0.75\psi_c = \psi_p$ is the best choice (see Fig. 6) for if this angle is used then the interpolation functions shape is quite similar to the original weight function (see Fig. 8). So finally the field can be reconstructed by

$$\mathbf{B}(\mathbf{z}) = \begin{cases} \sum_{m=0}^{M} \mathbf{C_m^{l,r}} \left(\frac{\mathbf{z} \pm a}{R_0}\right)^m, & \psi \le \psi_p \\ \mathbf{B_i}(\mathbf{z}), & \psi > \psi_p \end{cases}$$

$$\psi = \mathrm{Im}(\mathbf{cosh}^{-1}(\mathbf{z}/e)). \tag{52}$$

The circular multipole coefficients are then calculated as described in Section 2.3.1 using this reconstructed field.

The elliptic and circular coefficients were now checked interpolating the field on the ellipse and comparing it to the data used for calculating the coefficients. The interpolation error $\delta B_y +$

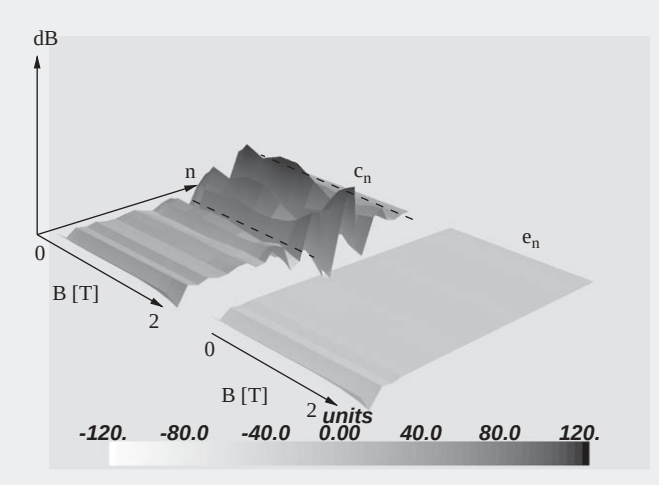

Fig. 10. The real part of the elliptic and circular multipole coefficients for different field levels. The biggest coefficients of the $e_n = 2 \times 10^4 E_n/E_1$ are found within the leading terms while the circular coefficients c_n show certain bands (indicated by dashed lines).

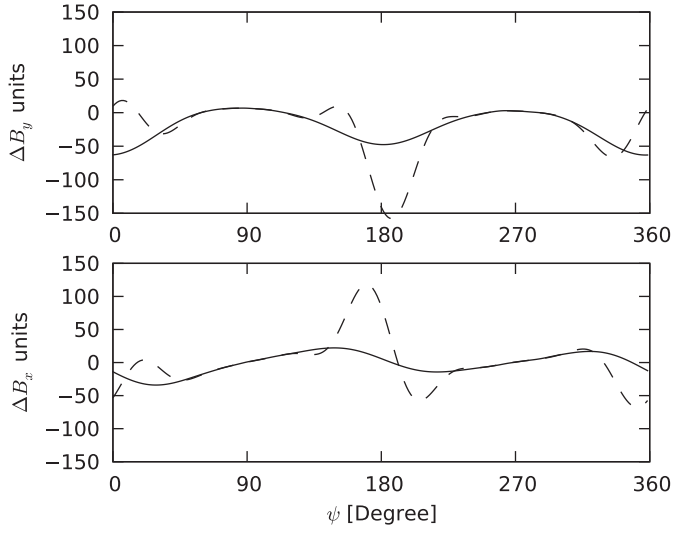

Fig. 11. The field as recalculated from the measurement using the elliptic multipoles and using eight circular multipoles. The solid line shows the field as reconstructed using the elliptic multipoles and the dashed line as reconstructed using 10 circular multipoles. One can see that the artefacts are nearly as large as the field inhomogeneity itself.

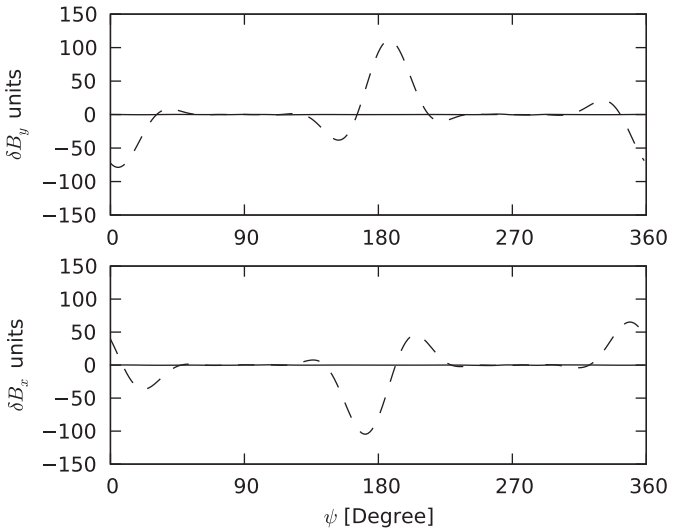

Fig. 12. The field interpolation errors for the elliptic (solid line) and circular field (dashed line) representation. Eight elliptic terms were used and ten circular terms. The circular multipoles produce artefacts which are larger than the field inhomogeneity itself.

$\delta iB_x = \delta \mathbf{B}_z(\mathbf{z})$ was defined to

$$\delta \mathbf{B_z}(\mathbf{z}) = \frac{10^4}{\mathbf{C_1}} \left[\mathbf{B}(\mathbf{z}) - \sum_{m=0}^{M} \mathbf{C_m} \left(\frac{z}{R}\right)^m \right] \tag{53}$$

for the circular multipoles with M the last used coefficient and to

$$\delta \mathbf{B_z}(\mathbf{z}) = \frac{2 \times 10^4}{\mathbf{E_0}} \left[\mathbf{B}(\mathbf{z}) - \frac{\mathbf{E_0}}{2} - \sum_{n=1}^{N} \mathbf{E_n} \cosh(n\mathbf{w}) \right]$$

$$\mathbf{w} = \mathrm{Arccosh}(\mathbf{z}/e) \tag{54}$$

for the elliptic multipoles with N the largest used coefficient. Fig. 9 demonstrates that both sets can reproduce the field with an acceptable quality. The circular multipoles produce artefacts at the edge of the ellipse if seven multipoles are used while the elliptic ones describe the fields with nearly no artefacts. Using 30 multipoles one can reach a field description as obtained using eight elliptic coefficients (see also Fig. 9).

Even if both sets are able to represent the field with sufficient accuracy the elliptic ones are easier to handle as the elliptic ones get smaller with higher order (see Fig. 10). The circular ones on the other hand produce bands of alternating coefficients. If one now cuts the sum within such a band larger artefacts can be created. To demonstrate this, the field was calculated on the ellipse again for 10 multipoles which were calculated using the first eight elliptic multipoles as described in Section 2.3.1. The reconstructed field is given in Fig. 11 and compared to the one used for obtaining the coefficients (see also Fig. 12). One can see that the artefacts are larger than the field distortion of the magnet itself. Similar effects were also observed for the coefficients calculated for the central field. This clearly shows that the elliptic coefficients are more adapted to describe magnetic fields within an ellipse, but circular multipoles can be still used if the truncation of the series is made with care.

5. Conclusions

(1) Within a circular domain a plane static magnetic field may be represented as a complex function, which may be expanded w.r.t. a complete set of circular multipoles. The expansion coefficients may be derived using a Fourier expansion from such a field given along the reference circle bounding this area.

(2) It is shown that a corresponding expansion may be done in an elliptic domain bounded by a reference ellipse. Expressions for the expansions coefficients for the elliptic multipoles are given comprising the field values given along the boundary. The completeness of this new set of elliptic multipole functions is shown.
(3) The circular and the elliptic expansion coefficients belonging to the same complex magnetic field are related to each other by linear transformations such that M coefficients of one set determine those of the other set in a unique way. General expressions for the elements of these triangular transformation matrices are given. If the aspect ratio of the ellipse gets larger, elliptic multipoles of a certain amplitude will be converted to larger circular multipoles than for an ellipse with a smaller aspect ratio. The elliptic multipoles usually provide a more accurate field description than the circular multipoles for the same number of coefficients.
(4) An elliptic reference curve fitting into a rectangular gap surrounds a larger area than a circular one matched to the same gap. This entails an advantage of the elliptic multipole expansion since the convergence and stability of each type of expansion is assured mainly within the corresponding reference curve.
(5) We demonstrated the validity of the elliptic and circular coefficients for the two-dimensional field of the curved single layer dipole with 8 turns (CSLD-8b). We showed that only these sets allow to reconstruct the field with a precision of better than 1 unit within the ellipse. Thus the circular multipole coefficients, obtained using the transformation from the elliptic ones, differ significantly from the circular multipoles, obtained from the data on the circle.
(6) A guide was given on how to interpret the data comparing the CSLD-8b design to the 10 turn single layer dipole as proposed in Ref. [11]. The plots of the multipoles versus the current clearly show that the first design provides a better field quality than the second one.
(7) The theory was applied for measurements performed using rotating coil probes. An analysis of the obtained coefficients shows that the largest elliptic coefficients of the series are found in the first ones while for the circular multipoles bands of large alternating coefficients are found. If the series is truncated within such a band, the field representation will contain large artefacts. This clearly shows that the elliptic coefficients are more adapted to describe magnetic fields within an ellipse, but circular multipoles can be still used if the truncation of the series is made with care.

References

[1] A.K. Jain, Basic theory of magnets, in: S. Turner (Ed.), CAS Magnetic Measurement and Alignment, no. 98-05 in CERN Yellow Reports, CERN, 1998, pp. 1–21.
[2] P. Schnizer, B. Schnizer, P. Akishin, E. Fischer, Magnetic field analysis for superferric accelerator magnets using elliptic multipoles and its advantages, in: The 20th International Conference on Magnet Technology, IEEE Transactions on Applied Superconductivity, vol. 18, 2008, pp. 1605–1608.
[3] S. Großmann, I. Funktionalanalysis, Akademische Verlagsgesellschaft, Frankfurt, Main, 1970, p. 82.
[4] P. Moon, D.E. Spencer, Field Theory Handbook: Including Coordinate Systems, Differential Equations and their Solutions, Springer, Berlin, 1988.
[5] P.M. Morse, F.H. Feshbach, Methods of Theoretical Physics, McGraw-Hill Book Comp., 1953.
[6] E. Madelung, die mathematischen Hilfsmittel des Physikers, Springer, Berlin, 1957, p. 225.
[7] O.D. Kellog, Foundations of Potential Theory, Frederick Ungar Publ. Comp., New York, 1929, p. 213.
[8] S. Gradshteyn, I. Ryzhik, Table of Integrals, Series and Products, Academic Press, New York, 1965.
[9] F.R. Peña, G. Franchetti, Elliptic and circular representation of the magnetic field in SIS 100, Technical Report ACC-note-2008-0001, GSI Helmholtzzentrum für Schwerionenforschung mbH, January 2008.
[10] E. Fischer, H. Khodzhibagiyan, A. Kovalenko, Full size model magnets for the FAIR SIS 100 synchrotron, in: The 20th International Conference on Magnet Technology, IEEE Transactions on Applied Superconductivity, vol. 18, 2008, pp. 260–263.
[11] A. Kovalenko, E. Fischer, H. Khodzhibagiyan, Cable in conduit and thermal budget at nuclotron, in: A CARE-HHH-AMT Workshop on Heat Generation & Transfer in Superconducting Magnets, LPNHE—Universite Pierre & Marie Curie (Paris VI) 4, Place Jussieu—75006 Paris, 2007.
[12] E. Fischer, et al., Manufacturing of the first full size model of a SIS100 dipole magnet, in: WAMSDO Workshop Proceedings, European Organization for Nuclear Research Report, no. 2009-001 in CERN Yellow Reports, CERN, 2009, pp. 147–156.
[13] G. Sikler, et al., Full size model manufacturing and advanced design status of the SIS100 main magnets, Presented at the WAMSDO Workshop at CERN, May 2008.
[14] E. Fischer, H. Khodzhibagiyan, A. Kovalenko, P. Schnizer, Fast ramped superferric prototypes and conclusions for the final design of the SIS 100 main magnets, in: Applied Superconductivity Conference ASC08, IEEE Transactions on Applied Superconductivity, 2008.
[15] E. Fischer, P. Schnizer, R. Kurnyshov, B. Schnizer, P. Shcherbakov, Numerical analysis of the operation parameters of fast cycling superconducing magnets, in: Applied Superconductivity Conference ASC08, IEEE Transactions on Applied Superconductivity, 2008.
[16] P. Schnizer, et al., Mole for measuring pulsed superconducting magnets, in: The 20th International Conference on Magnet Technology, IEEE Transactions on Applied Superconductivity, vol. 18, 2008, pp. 1648–1651.
[17] A.K. Jain, Harmonic coils, in: S. Turner (Ed.), CAS Magnetic Measurement and Alignment, no. CERN 98-05 in CERN Yellow Reports, CERN, 1998, pp. 175–217.
[18] P. Schnizer, Measuring system qualification for LHC arc quadrupole magnets, Ph.D. Thesis, Graz Technical University, Geneva, CERN-THESIS-2003-006, 2002.